Applied Catalysis B: Environmental 90 (2009) 55–63

Contents lists available at ScienceDirect

Applied Catalysis B: Environmental

journal homepage: www.elsevier.com/locate/apcatb

3-D ordered mesoporous KIT-6 support for effective hydrodesulfurization catalysts

K. Soni [a], B.S. Rana [a], A.K. Sinha [a,*], A. Bhaumik [b], M. Nandi [b], M. Kumar [a], G.M. Dhar [a,*]

[a] Indian Institute of Petroleum, Mohkampur, Dehradun 248005, India
[b] Indian Association for Cultivation of Science, Kolkata, India

ARTICLE INFO

Article history:
Received 30 October 2008
Received in revised form 12 February 2009
Accepted 17 February 2009
Available online 25 February 2009

Keywords:
Mesoporous
Hydrodesulfurization

ABSTRACT

KIT-6 silica with well-ordered 3-D mesoporosity was developed as support for Mo, CoMo and NiMo catalysts. TEM and low-angle XRD analyses were used to ensure that the cubic Ia3d mesostructure is stable after Mo and promoter incorporation. The wide-angle XRD (as well O_2-chemisorption analysis) was used to verify MoO_3 (and MoS_2) dispersion, with crystallite size <40 Å. The IR spectral studies were used to determine the nature of Mo species (octahedral and tetrahedral) and their growth with increasing Mo loading. TPR studies were also used to understand the nature of Mo species and their reducibility. A linear correlation was obtained between catalytic activities and oxygen uptakes suggesting that the increase in anion vacancies were responsible for the observed variation of hydrodesulfurization and hydrogenation activities. A comparison with γ-Al_2O_3 and SBA-15 supported catalysts shows superior activities of KIT-6 supported catalysts which is attributable to 3-D mesopore connectivity resulting in better catalyst dispersion, higher reducibility of Mo, and faster diffusion of reactant and products in the KIT-6 supported catalysts.

1. Introduction

Strict emission reduction legislations for sulfur and nitrogen compounds will require more severe hydrodesulfurization (HDS) and hydrodenitrogenation (HDN) of petroleum fraction. Therefore, present day catalysts and operating conditions will have to be adapted to new requirements. Development of more active HDS catalysts is one of the main goals of the refining industry. Such a demanding task requires catalysts that are several times more active than the present catalysts [1] in order to achieve 5 ppm sulfur in diesel. It is not only the high activity but they should also have different activity profiles with respect to different functionalities. In order to modify the activity to achieve the above said objectives several approaches have been pursued among which variation of support is an important one [2–4].

γ-Al_2O_3 is the only support used in commercial HDS catalysts. Many other supports have been tried with considerable success. Among them clays [5], carbon [6], oxides [7–10], mixed oxides [11–17], zeolites [18,19] and mesoporous materials like MCM-41 [20–23], HMS [24] and SBA-15 [25] have been studied. SBA-15 supported CoMo and NiMo catalysts are reported to exhibit higher activities for conversion of thiophene than γ-Al_2O_3. Vradman et al. [26] reported higher activities for HDS and hydrogenation (HYD) using NiW/SBA-15 catalysts. Kumaran et al. [27,28] reported on Al-SBA-15 of various Si/Al ratio for HDS of thiophene and suggested that Al containing SBA-15 supported catalysts displayed higher activities than the γ-Al_2O_3 supported catalysts. Chiranjeevi et al. [29] reported the same for Al-HMS supported Mo catalysts.

Reddy et al. [30] showed that MCM-41 can be used as effective support for hydrodesulfurization catalysts. Sampieri et al. [31] prepared MoS_2/SBA-15 and MoS_2/MCM-41 catalysts with various Mo loading by mechanical mixing followed by thermal spreading without serious damage to the support structure. For SBA-15 supported catalyst the MoS_2 slabs appeared to be oriented at random in the porosity of the support and an average MoS_2 slab length of 2.8 nm and a stacking of 2 was determined. But for MCM-41 supported catalysts, MoS_2 slabs blocked the relatively smaller mesopores resulting in comparatively lower activity than for SBA-15 supported counterparts. Corma et al. [32] have reported that mesoporous aluminosilicate MCM-41 is a good catalyst for carrying out mild hydrocracking of vacuum gas oil. A combination of large surface area, uniform pore-size distribution large enough to allow diffusion of large molecules, together with the presence of mild acidity and high stability, result in superior HDS, HDN and hydrocracking performance than zeolite and alumina supported catalysts.

We studied a 3-D mesoporous silica (KIT-6) support to develop catalyst for HDS and HYD of liquid fuels. Recently, cubic mesoporous silica with larger than 5 nm size pores have attracted

* Corresponding authors. Fax: +91 135 266 203.
E-mail addresses: asinha@iip.res.in (A.K. Sinha), dhargm@gmail.com (G.M. Dhar).

0926-3373/$ – see front matter © 2009 Elsevier B.V. All rights reserved.
doi:10.1016/j.apcatb.2009.02.010

much attention for potential applications in catalysis. Ryoo and co-workers [33] reported a new synthesis route to high quality cubic, mesoporous Ia3d silica, KIT-6, using copolymer ($EO_{20}PO_{70}EO_{20}$)–butanol mixture. This mesoporous silica, KIT-6 possesses large readily tunable pores with thick pore walls, high hydrothermal stability, high specific surface area and large pore volume. These materials are expected to be superior to mesoporous structures with one or two-dimensional channels due to better dispersion of catalyst and faster diffusion of reactants and products during reaction in the 3-D interconnected mesopores.

In this present work with the aim of increasing the HDS activity for molybdenum catalysts, we prepared KIT-6 mesoporous support for HDS catalysts. The support and catalysts were characterized by several techniques. Catalytic evaluations for HDS of thiophene and HYD of cyclohexene were carried out on pre-sulfided catalysts. Comparison of HDS activity was done with commercial γ-Al_2O_3 and SBA-15 supported catalysts to emphasize the efficacy of KIT-6 supports.

2. Experimental

2.1. Synthesis

KIT-6 material was prepared by following the published procedure [33] using a triblock copolymer (P123, Sigma-Aldrich) poly (ethylene oxide)–poly (propylene oxide)–poly (ethylene oxide) as structure directing agent. In a typical synthesis, 6 g P123 was dissolved in 217 g of distilled water and 11.8 g of concentrated HCl (35%), to this 6 g of 1-butanol was added under stirring at 35 °C. After 1-h stirring 12.9 g of TEOS was added dropwise at 35 °C. The mixture is stirred for 24 h at 35 °C. The final solution is transferred to a Teflon bottle and heated at autogeneous pressure for 24 h at 100 °C. The solid product obtained after hydrothermal treatment was filtered and dried at 100 °C without washing. The template was removed by extraction in an ethanol–HCl mixture, followed by calcinations at 550 °C.

The molybdenum supported catalysts were prepared by incipient wetness impregnation method using KIT-6 material as support and appropriate amount of ammonium heptamolybdate. The Co and Ni promoted catalysts were prepared by impregnating the promoter using their nitrate salts over Mo impregnated catalysts. The impregnated catalysts were dried in an oven at 100 °C overnight followed by calcination at 550 °C for 6 h. For comparison γ-alumina and mesoporous SBA-15 supported catalysts with similar composition were prepared as described in detail in earlier publications [25].

2.2. Characterization

The catalysts and support were characterized by X-ray diffraction (XRD), nitrogen-sorption analysis, transmission electron microscopy (TEM), energy dispersive X-ray (EDX) analysis, electron spectroscopy for chemical analysis (ESCA), temperature programmed reduction (TPR), Fourier transform infrared spectroscopy (FT-IR), and low temperature oxygen chemisorption (LTOC). XRD pattern were obtained using Cu Kα radiation (40 kV and 40 mA). The porous properties of KIT-6 and metal loaded catalysts were examined by N_2 adsorption–desorption isotherms at 77 K and the related data (surface area, S_{BET}; pore volume, V_P; pore diameter, D_p) were calculated. IR analyses were carried out by mixing the powder sample with KBr and making it into a thin wafer of 13 mm diameter. Each sample was scanned for 20 times at a resolution of 2 cm^{-1}, and the average spectrum was taken. The TPR profiles were obtained using a TPD/TPR-2720 Micromeritics (USA) instrument for analyzing the nature of reducible metal species present in the samples. TPR profiles were taken from ambient temperature to 1000 °C (10 °C/min), and then the temperature was kept isothermal for 30 min. A 10% H_2/Ar mixture at a flow rate of 25 ml/min was used as reducing gas. The hydrogen consumption corresponding to the reduction of metal oxide at various stages of reduction was computed from the peak area calibrated with a standard Ag_2O sample. The oxygen uptake were measured at −78 °C for the catalysts sulfided at 400 °C for 2 h using a CS_2/H_2 mixture at a flow rate of 40 ml/min, according to the procedure reported by Parekh and Weller [34] for reduced molybdenum catalysts. Oxygen chemisorption data were used to calculate various parameters such as equivalent molybdenum sulfide area (EMSA), surface coverage and crystallite size using the following formulas:

EMSA = O_2 uptake × 0.566616 (this value is obtained from pure MoS_2 surface area divided by oxygen uptake, based on the inverse site density for MoS2 as reported in earlier literature [35,36]).

Surface coverage = 100 × (EMSA/surface area).

Crystallite size = $5 \times 10^4/(F \times M)$, where F is density of MoS_2 (4.8 g/ml) and M is the EMSA/(g of MoS_2).

2.3. Catalytic activities

Thiophene HDS and cyclohexene HYD were carried out at 400 °C on the catalysts sulfided at the same temperature for 2 h in flow of CS_2/H_2 mixture, in a fixed bed reactor operating at atmospheric pressure. The reactants and products were analyzed on-line by gas chromatography (GC) (Chemito, FID, 10% OV-17 packed column). The reactor and GC were interfaced using a six-way sampling valve [37]. First order rates were evaluated according the equation $x = r\ (w/f)$ where r is the rate in moles per hour per gram, x is the fractional conversion, w is the weight of the catalyst in grams and f is the flow rate of the reactant in moles/hour. The rates calculated for HDS and HYD reaction are taken as a measure of their respective activities. The conversions were kept below 15% to avoid pore-diffusion limitations.

3. Result and discussion

3.1. Characterization of support and supported catalysts

3.1.1. X-ray analysis

The low angle X-ray diffraction pattern of the calcined KIT-6 is displayed in Fig. 1. The XRD pattern shows a sharp intense peak at $2\theta = 1.06$ correspoding to (2 1 1) plane and a hump for (2 2 0) plane. The XRD pattern clearly indicates that material is well ordered mesoporous and belongs to bicontinuous cubic space group Ia3d [38]. The unit cell parameter a_0 of calcined sample was calculated to be 203.9 Å (2 1 1) and 177 Å (2 2 0) in good agreement with literature and suggests that mesoporous silica is KIT-6 with body centered cubic symmetry. Fig. 1 also shows low-angle XRD patterns of Co and Ni promoted catalysts. The XRD patterns clearly shows the long range 3-D cubic symmetry of the space group Ia3d, with sharp peak due to the (2 1 1) reflection. The unit cell parameter calculated from $a_0 = 6^{1/2}d_{2\,1\,1}$ is 203.9 Å. The similarities in X-ray diffraction peaks suggest that the mesoporous cubic structure is retained even after metal loading.

Various catalysts containing different amounts of Mo supported on KIT-6 were examined by X-ray diffraction in the region, where MoO_3 peaks appear. The results reveal that MoO_3 is well dispersed up to 8 wt.% Mo loading (X-ray invisible) and probably present as a monolayer, but beyond this loading MoO_3 aggregation to larger particles started. The diffractograms of the catalysts with different Mo loading are shown in Fig. 2. It is important to note that there is

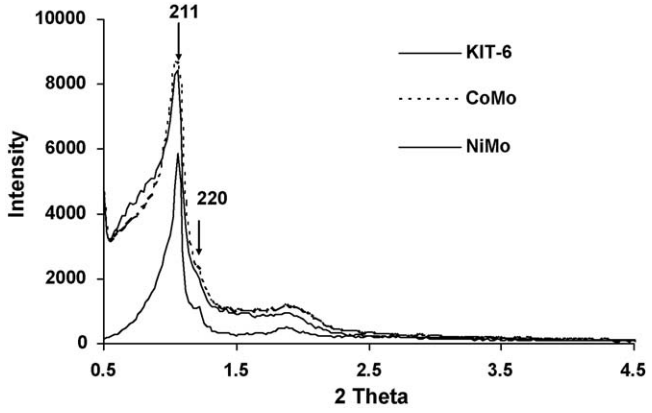

Fig. 1. Low-angle XRD Pattern of KIT-6 support catalysts.

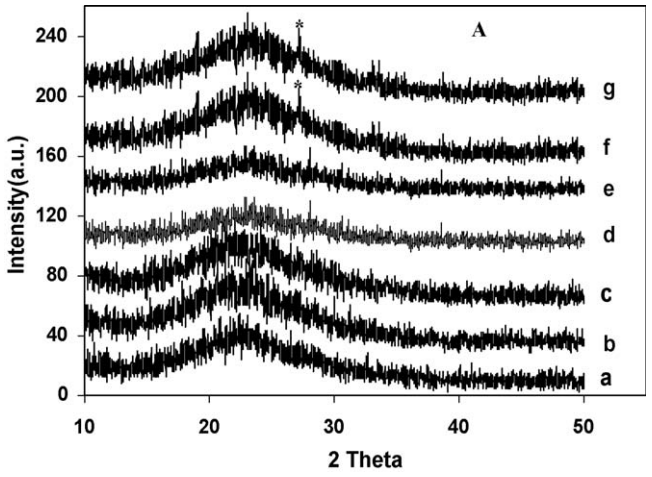

Fig. 2. Wide-angle XRD pattern of KIT-6 supported Mo catalysts (a) KIT-6, (b) 2%, Mo (c) 4% Mo, (d) 6% Mo, (e) 8% Mo, (f) 10% Mo and (g) 12% Mo.

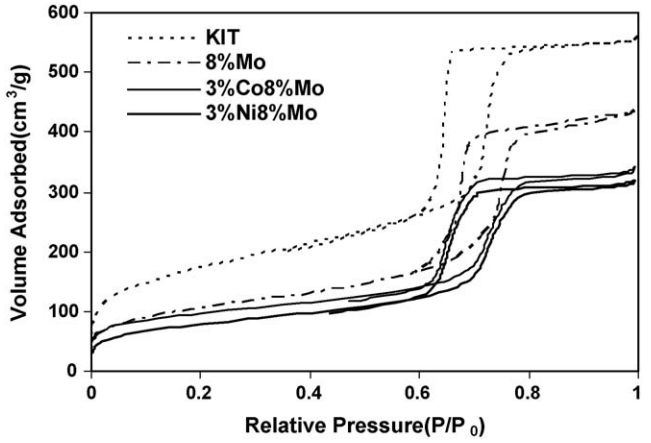

Fig. 3. N_2 adsorption–desorption isotherms of KIT-6 supported Mo and CoMo and NiMo catalysts.

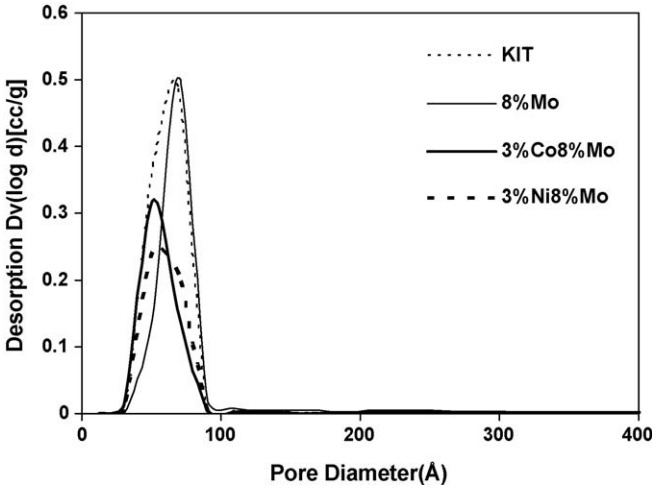

Fig. 4. Pore-size distribution of KIT-6 supported Mo and CoMo catalysts.

no indication of the presence of crystalline MoO_3 up to 8 wt.% Mo which suggests that MoO_3 is well dispersed on KIT-6 up to 8 wt.% loading. The absence of XRD signals indicates that the particle size of MoO_3 is below the coherence length of X-ray scattering i.e. smaller than ~30–40 Å up to 8 wt.% Mo. At higher Mo loadings evidence for the crystalline MoO_3 can be seen as a weak signal at $2\theta = 27.3^\circ$. There is no indication of the presence of crystalline sulfide phase up to 8 wt.% Mo for the sulfided/reaction-aged catalysts

3.1.2. N_2 sorption analysis

The porous properties of KIT-6 and metal loaded catalysts were examined by N_2 adsorption–desorption isotherms at 77 K. The N_2 adsorption–desorption isotherms are shown in Fig. 3 and the related data (surface area S_{BET}, pore volume V_P, pore diameter D_p, unit cell parameter a_0 and pore wall thickness δ) are presented in Table 1. It can be seen that calcined mesoporous Ia3d silica support and metal loaded catalysts show type-IV isotherm with H_1-type hysteresis loop and a sharp capillary condensation step in the 0.6–0.8 P/P_0 range, indicative of large channel like pores with a narrow range pore-size distribution. A narrow pore-size distribution with mean value 70 Å calculated from the adsorption isotherm using BJH method is shown in Fig. 3. The mean pore diameter is more or less constant after Mo loading but decreases after promoter loading (Fig. 4). No changes were detected in the nature of isotherm or in the shape of the hysteresis loop indicating that the support pore structure is preserved after Mo and promoter deposition. But the height of the hysteresis loop decreased after Mo loading due to decrease in the pore volume resulting from metal loading in the mesopores. Significant decrease in surface area (S_{BET}) and pore volume are observed when Mo and Co or Ni are incorporated in the support (Table 1).

Table 1
Textural characterization of KIT-6 supported 8% Mo and 3% Co, 8% Mo and 3% Ni, 8% Mo catalysts.

Sample	S_{BET} (m^2/g)	S_{EXT} (m^2/g)	S_{MIIC} (m^2/g)	V_T (cm^3/g)	V_{MESO} (cm^3/g)	V_{MIC} (cm^3/g)	Mean poredia (Å)	a_0[a] (Å)	δ[b] (Å)
KIT-6	625	547	77	0.86	0.70	0.026	70.1	203.9	144.3
8% Mo/KIT	374	334	40	0.67	0.59	0.014	70.0	–	–
3% Co, 8% Mo/KIT	275	231	43	0.49	0.43	0.017	50.8	203.9	153.1
3% Ni, 8% Mo/KIT	281	253	37	0.49	0.43	0.014	50.5	203.9	153.4

[a] Unit cell parameter estimated from the position of the (2 1 1) diffraction line ($a_o = 6^{1/2} d_{2\,1\,1}$).
[b] Pore wall thickness ($\delta = a_0 - D_p$).

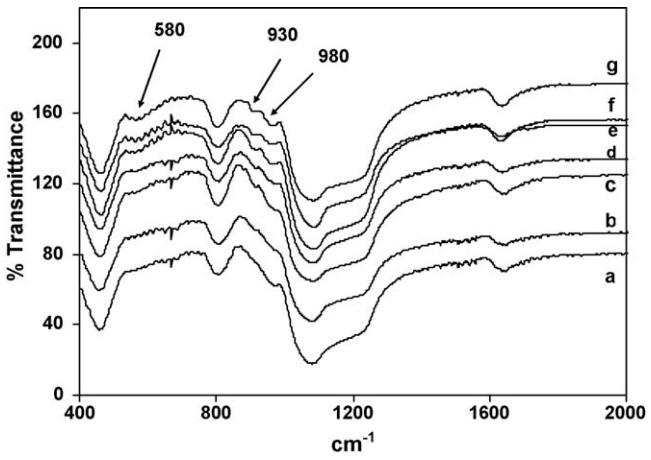

Fig. 5. FT-IR spectra of KIT-6 supported Mo catalysts (a) KIT-6, (b) 2% Mo, (c) 4% Mo, (d) 6% Mo, (e) 8% Mo, (f) 10% Mo and (g) 12% Mo-KIT-6.

3.1.3. FT-IR spectroscopy

Infrared spectra are useful to ascertain the presence of various molybdates. The IR spectra of KIT-6 and Mo/KIT-6 with varying Mo loading are shown in Fig. 5. The framework region spectrum of KIT-6 consists of bands centered at ~1085, 799 and 1660 cm^{-1}. The 1085 cm^{-1} band is attributed to T–O asymmetric stretching vibrations and the band at 800 cm^{-1} is due to T–O symmetric stretching vibrations due to intrinsic vibration of TO_4 tetrahedra of silica. These bands are generally structure sensitive but are also dependent on the composition. Introduction of Mo into the structure creates new features around 930, 980 and 580 cm^{-1}. These features increase in intensity with increase in molybdenum loading. The features in this region are generally attributed to tetrahedral, octahedral, and other polymolybdates and crystalline MoO_3 [39]. The bands between 1085 and 799 cm^{-1} appear to be due to octahedral and tetrahedral molybdenum species. The vibrations due to Mo tetrahedral species appear at 930–830 cm^{-1} and for octahedral and other polyhedral species appear in 990–930 and 860–800 cm^{-1}. These spectral studies provide evidence for the presence and growth of tetrahedral and octahedral molybdenum species on these KIT-6 supported catalysts. The characteristic band of bulk MoO_3 normally appears at 820 cm^{-1}. This band overlaps with broad 813 cm^{-1} band, therefore the presence of crystalline MoO_3 is difficult to ascertain from IR studies alone. Similar results are also presented by Kumaran et al. [28]. IR has been reported to be used complementarily to characterize molybdenum species [40,41] supported on silica [42] The low-frequency range 600–1100 cm^{-1} has been ascribed to absorptions due to molybdate species and silica bands (1100 and 800 cm^{-1} for SiO_2). Polymolybdate species are known to exhibit absorption bands at 975 and 885 cm^{-1}, MoO_3 at 998 and 870 cm^{-1}. For low Mo content the band at 975 cm^{-1} has been observed alone indicating that molybdate species are present while MoO_3 is not. For high Mo content the bands at 975 and 885 cm^{-1} due to polymolybdate species and at 998 cm^{-1} due to MoO_3 were observed all together. If reduction by hydrogen or methanol was performed at 200 °C the

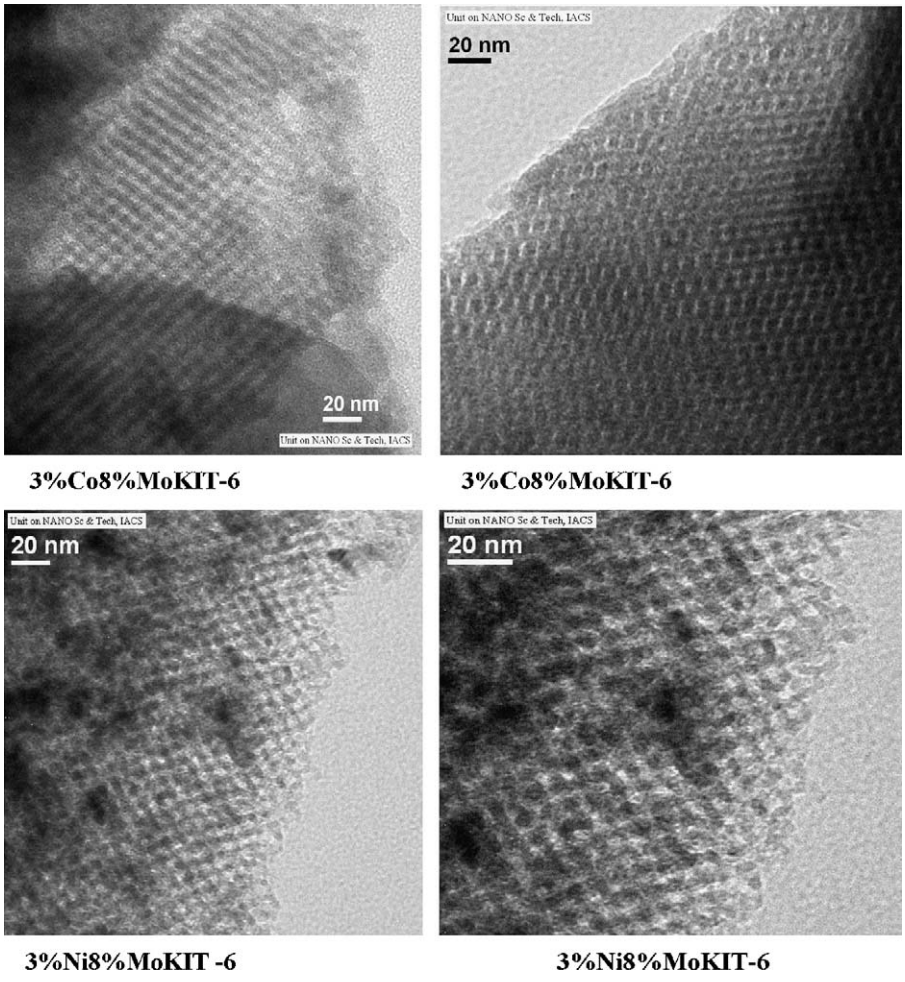

Fig. 6. TEM graphs of CoMo and NiMo catalysts supported KIT-6 material.

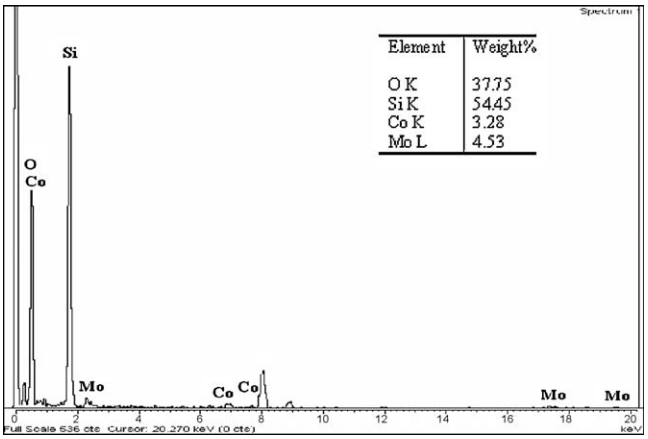

Fig. 7. EDX pattern of KIT-6 supported CoMo catalysts.

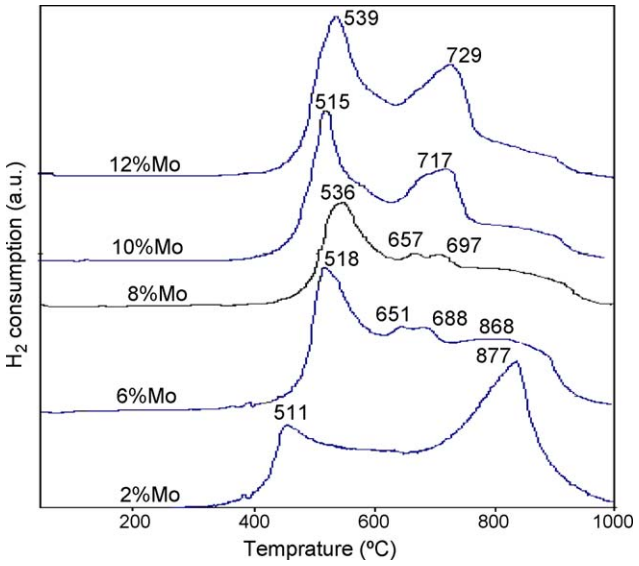

Fig. 8. TPR profiles of KIT-6 supported molybdenum catalysts.

998 cm^{-1} band disappeared while the other two remained. This indicates that the covalency of the Mo═O bands decreased due to the reduction of MoO_3 particles [43].

3.1.4. TEM/EDAX and XPS analysis

Fig. 6 presents the TEM of the 3% Co–8% Mo/KIT-6 and 3% Ni–8% Mo/KIT-6. TEM was performed to analyze the mesoporous structure of the samples and dispersion of the catalysts on support. A well-ordered cubic array of mesopores is observed for these samples and the centers of two adjacent pores are about 100 Å apart and the pore diameter is about 60 Å which are similar to the pore-size data obtained from nitrogen sorption analysis. High resolution TEM did not show presence of any significant metal oxide agglomerates on the support surface indicating that the catalyst is well dispersed on the support surface and in the mesopores. This observation is also supported by the absence of any crystalline MoO_3 phase in the XRD pattern. EDX results are also shown in Fig. 7. Through the qualitative local EDX analysis, we can verify that the nanoparticles finely dispersed on the support, are composed of Co and O which form a uniform over-layer on the dispersed Mo oxide. The atomic wt.% of Co and Ni, calculated by EDX analysis are similar to actual Co and Ni deposited but the amount of Mo from EDX analysis is lower (nearly half) than the actual Mo loading which could be due to non-uniform distribution of Mo resulting in lower Mo from local EDX analysis than the actual loading. Mo loading on support surface from XPS analysis is nearly similar to the actual loading (Table 4).

HRTEM of sulfided catalyst (8% Mo) (Supporting Fig. 2) showed presence of only few particles with up to 2-layer stacks of MoS_2 with 0.6 nm line spacing. But majority of particles are present as monolayer. At higher loading (10% Mo) 3–4-layer stacks with larger particles are observed indicating three-dimensional growth of MoS_2 at higher loadings.

3.1.5. Temperature programmed reduction (TPR)

TPR profiles of samples containing 0–12 wt.% Mo are shown in Fig. 8. One main reduction peak appearing around 500 °C is observed which can be assigned to the first reduction step of $Mo^{6+} \rightarrow Mo^{4+}$ of polymeric octahedral Mo species weakly bound to the silica surface [44,45]. Another peak at about 800 °C observed in the TPR pattern of Mo/SiO_2 samples can be assigned to the reduction step $Mo^{+4} \rightarrow Mo^0$ or to the first step of reduction of isolated tetrahedral Mo^{+6} species in strong interaction with silica support [43,46]. These results indicate that at least two types of molybdenum species are present on the catalyst surface. At lower loading, MoO_3 is mostly present as tetrahedral species, which is difficult to reduce due to strong interaction with support. It is clear that with increase in Mo loading, the concentration of easily reducible octahedral species increases. Similar results have been observed for Mo-oxo species supported on Al-SBA-15 [28].

Table 2
TPR data of KIT-6 supported molybdenum catalysts.

Wt.% Mo	Reduction temperature (°C)		Hydrogen consumption (ml), STP		
	T_{1max}	T_{2max}	Per gram catalyst	Per gram Mo	H_2/Mo[a]
0	–	–	–	–	–
2	511	–	1.3	66.5	0.57
6	518	688	7.9	132	1.14
8	536	697	14.9	186	1.61
10	515	717	19.3	193	1.67
12	539	729	24.2	202	1.74

[a] Molar ratio.

The reduction temperature and the H_2 consumption data are given in Table 2. It is clear from the table and Fig. 9 that H_2 consumption increases continuously up to 8 wt.% Mo and there is little increase at higher loadings indicating maximum dispersion at 8 wt.% loading. H_2/Mo molar ratio less than theoretical value of 3.0 indicates that the reduction is not complete under the condition employed. However in the case of higher loading, the value

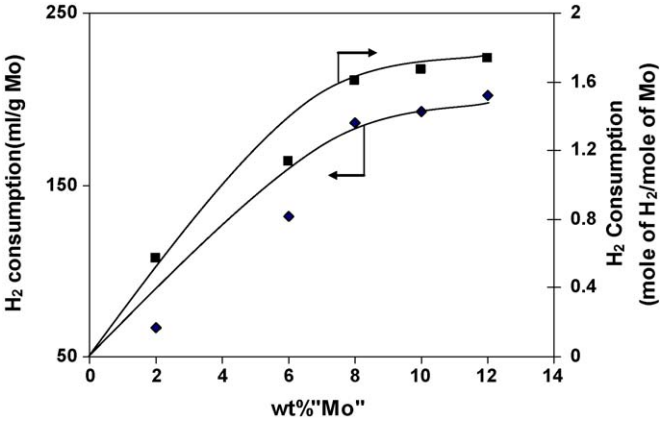

Fig. 9. Variation of H_2 consumption with Mo loading on KIT-6 supported catalysts.

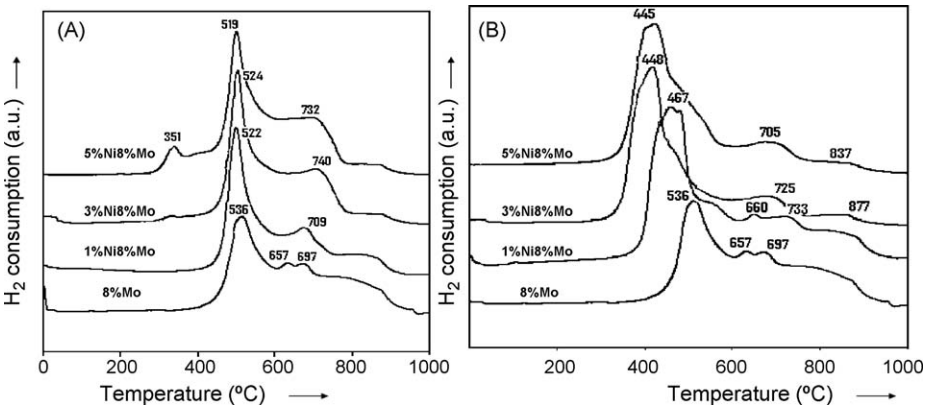

Fig. 10. TPR pattern of (A) Co and (B) Ni promoted molybdenum catalysts supported on KIT-6 support.

increases but is still lower than the theoretical value. The linearity of the hydrogen uptake with Mo loading detected in TPR experiments may not be direct evidence for "maximum dispersion" of Mo species and decreasing of H_2-uptake – for lower dispersion but they do give an idea about reducibility of Mo species – similar reducibility (% reduction) of Mo-species in loading range up to 8 wt.% and difficulties for their reduction at higher loading. One of the possible reasons for it can be blocking of supports pores with Mo-species at higher loadings. But the larger particle size at higher loadings could also be responsible for lower reducibility. Xiong et al. [47] reported a negative correlation between the Co_3O_4 particle size and the degree of reduction for γ-Al_2O_3-supported cobalt catalysts.

3.1.5.1. Effect of promoters on the reducibility of catalysts. The effect of Co and Ni promoters on the reducibility of catalysts have been shown in Fig. 10. The H_2 consumption data and reduction temperature profile have also been given in the Table 3. It can be seen that the reduction pattern of promoted catalysts shifted to the lower temperature side, suggesting that the promoters increase the reducibility of Mo species. Ni appears to be more effective compared to Co. The maxima of the main peak at 536 °C for 8% Mo KIT-6 (reduction of Mo-oxo species) is shifted by Ca 91 °C towards lower temperature for Ni promoted one. The main peak with maxima at 445 °C is associated with the reduction for both Mo-oxo species and NiO-oxo species (overlapping of MoO_3 and NiO reduction regions). The H_2 consumption per gram of Mo and H_2: Mo molar ratio indicates that 8 wt.% Mo sample is not completely reduced, whereas the addition of a promoter helps to increase the reducibility. For the addition of 3 wt.% Co or Ni to 8 wt.% Mo, however, H_2/Mo molar ratio is higher than the theoretical value of 3.0, indicating that promoter oxide reduction also contributes to total reduction at this stage.

Table 3
TPR data of Co and Ni promoted 8% Mo KIT-6 catalysts.

Wt.%	Reduction temperature (°C)	Hydrogen consumption (ml)	
		Per gram catalyst	H_2/Mo[a]
8% Mo	536, 657, 697	14.9	1.6
1% Co	522, 709, 843, 875	19.9	2.1
3% Co	524, 740	35.2	3.8
5% Co	351, 519, 732	41.0	4.4
1% Ni	467, 660, 733	23.0	2.5
3% Ni	448, 725, 877	34.7	3.7
5% Ni	445, 705, 837	41.1	4.4

[a] Assuming that only MoO_3 is undergoing reduction.

3.1.6. Low temperature oxygen chemisorption

Low temperature oxygen uptake was determined for supported sulfided catalysts at −78 °C. The corresponding data are plotted as a function of Mo content in Fig. 11. It is generally accepted that oxygen chemisorption is related to anion vacancies and it measures the general state of dispersion of molybdenum in sulfided condition [48]. The trend in the variation of oxygen chemisorption as a function of Mo loading suggests that dispersion of molybdenum increases up to 8 wt.% Mo loading and it decreases at higher loadings due to some agglomeration of the dispersed molybdenum sulfides. Similar behaviors have also been reported by Kumaran et al. [28]. Various parameters can be evaluated from oxygen chemisorption data such as EMSA, surface coverage and crystallite size [35,36], which are shown in the Table 4. The surface coverage can be attributed to the selective interaction of molybdenum with certain preferred area of support. It can be noted from the table that only 13.0% of the total surface is covered by molybdenum, indicating that molybdenum selectively interacts with some portion of support.

The crystallite size remains more or less constant up to 8 wt.% Mo (<30 Å) and beyond this loading there is a fast growth of MoS_2 crystallite size. O/Mo ratio which quantifies active metal dispersion can also be calculated from oxygen chemisorptions values, and it is plotted as a function Mo-loading in Fig. 12. The consistency of dispersion and crystallite size up to 8 wt.% Mo may be due to lateral growth of single molybdenum slabs as patches on various parts of the support and three-dimensional growth of crystallite may take place beyond this loading. Thus, it appears that

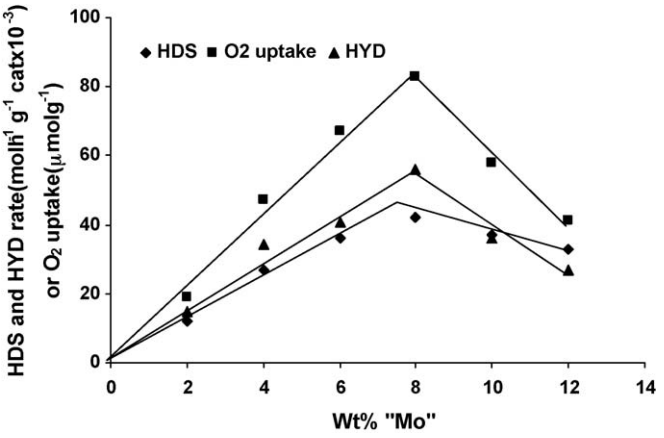

Fig. 11. Variation of catalytic activity and O_2 uptake with molybdenum loading on KIT-6 supports.

Table 4
BET surface area and oxygen chemisorption's data of KIT-6 supported molybdenum catalysts.

Mo (wt.%)	S_{BET} (m^2/g)	O_2 uptake (μmol/g)	O/Mo × 100	EMSA[a] (m^2/g)	% Surface coverage[b]	Crystallite size (Å)[c]
0	625					
2 (4.36)[x]	429	19.1	21.8	10.8	2.61	19.3
4 (6.57)	408	46.8	22.5	26.6	6.69	15.6
6 (7.85)	382	67.0	21.5	38.0	10.6	16.5
8 (10.7)	374	83.1	20.0	47.0	13.0	17.7
10 (11.2)	365	58.0	11.1	32.8	9.4	31.7
12 (14.2)	358	41.2	6.6	23.2	6.8	53.8

x = the Mo wt.% by XPS.
[a] EMSA = O_2 uptake × 0.566616 (this constant value is obtained from pure MoS_2 BET surface area divided by oxygen uptake).
[b] Surface coverage = 100 × (EMSA/surface area).
[c] Crystallite size: $5 \times 10^4/(F \times M)$, where *F* is density of MoS_2 (4.8 g/ml) and *M* is the EMSA/(g of MoS_2).

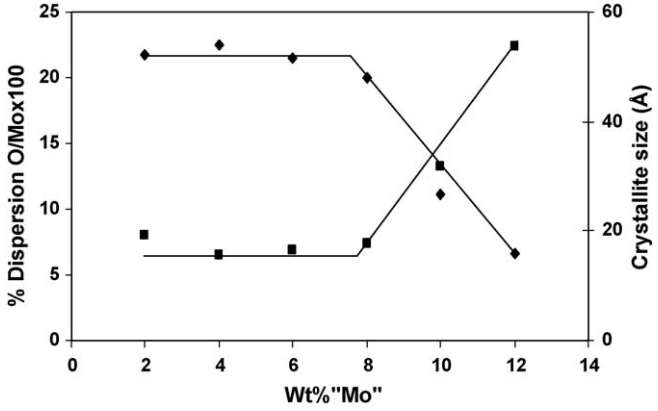

Fig. 12. Effect of Mo loading on % dispersion and crystallite size of KIT-6 supported Mo catalysts.

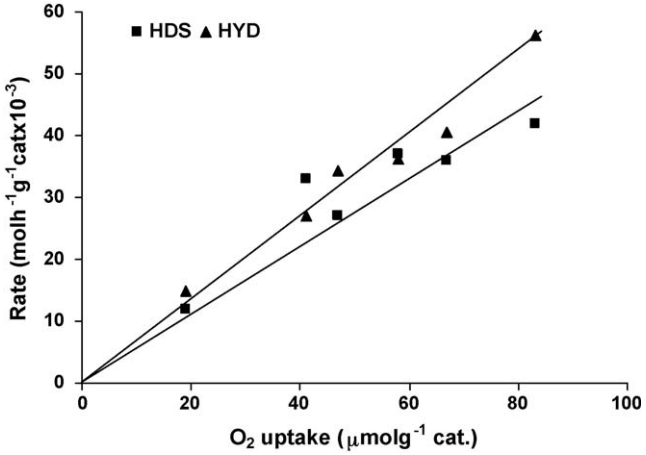

Fig. 14. Comparison between oxygen chemisorption and reaction rates of KIT-6 supported Mo catalysts.

molybdenum is well dispersed and probably present as monolayer patches up to 8 wt.% Mo loading.

3.2. Catalytic activity

Hydrodesulfurization of thiophene and hydrogenation of cyclohexene were carried out on molybdenum supported KIT-6 catalysts. It can be seen from Fig. 11 that HDS and HYD activity for Mo/KIT-6 increase up to 8 wt.% Mo and then decrease with further increase in Mo loading. These observations are very similar to the variation of oxygen chemisorption on the Mo supported catalysts. Therefore, it appears that there is a definite relationship between oxygen chemisorptions and catalytic functionalities.

Activities expressed as quasi turn over frequency (QTOF) (rate per unit amount of molybdenum) for HDS reaction and HYD reactions shown in Fig. 13 are more or less constant up to 8 wt.% Mo and with further increase in Mo content, activity decreases due to metal–metal interaction or larger crystal size. O/Mo ratio and QTOF show similar trend indicating that QTOF is dependent on dispersion. O/Mo is related to activity through anion vacancies which are the seat of activity measured by oxygen chemisorption.

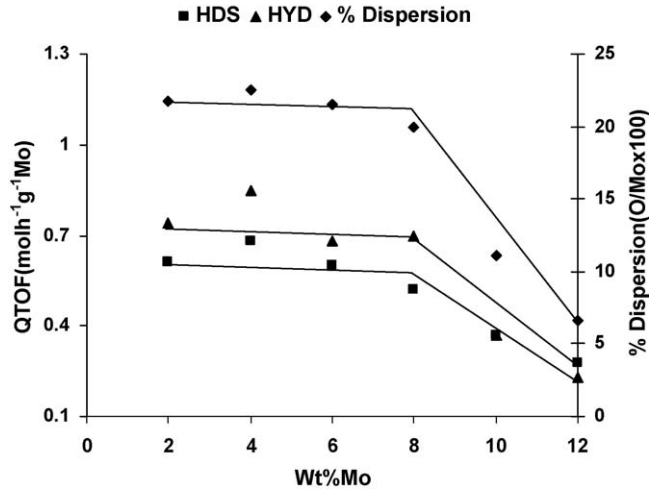

Fig. 13. Relationship between activity and % dispersion derived form O_2 uptake.

3.2.1. Correlation between oxygen chemisorption and catalytic activity

It is already mentioned that variation in oxygen chemisorption with metal loading is similar to the variation of the catalytic functionalities. In order to establish a clear relationship between these two parameters, the rate for each functionality (HDS and HYD) is plotted through origin against O_2 uptake (Fig. 14). A nearly linear relationship is obtained indicating that these catalytic activities are proportional to O_2 uptake.

3.2.2. Effect of promoter on activity

The promotional effects of Co and Ni on 8 wt.% Mo/KIT-6 catalysts are studied with variation of promoter concentration from 1 to 5 wt.% (Fig. 15). The promoted catalysts were tested for HDS and HYD reactions under similar condition. It can be seen that activity increases with promoter concentration up to 3 wt.% Co and Ni loading and decreases with higher loading. The variation in both the activities (HDS and HYD) (as well as O_2 uptake) show similar trend and this is probably due to the fact that Co or Ni promoters

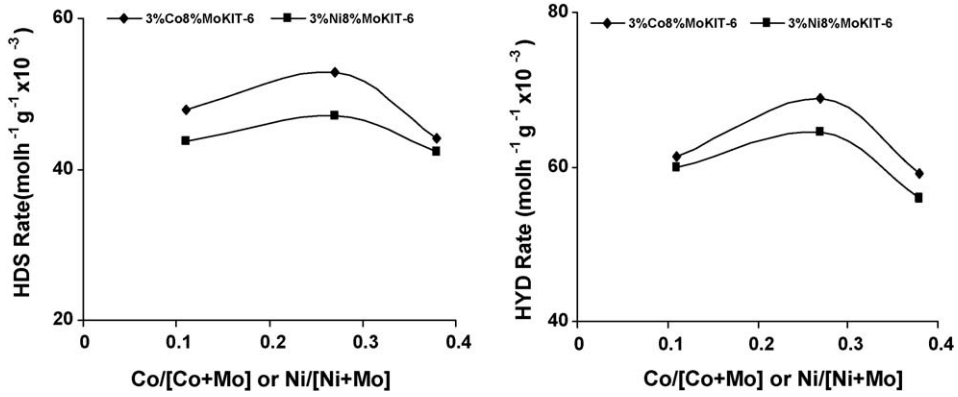

Fig. 15. Effect of Co and Ni content on HDS and HYD activity of KIT-6 supported Mo content.

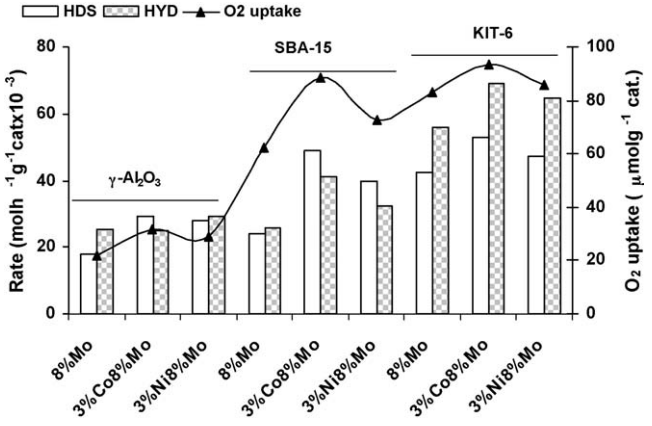

Fig. 16. Comparisons of HDS, HYD and O_2 uptake activities of Mo, CoMo and NiMo catalysts supported over γ-Al_2O_3, SBA-15 and KIT-6 materials.

(up to 3 wt.% loading) contribute to increase in anion vacancies, which are the sites for both type of activities [14].

3.2.3. Support effect on activity

It is interesting to compare the catalytic activities of Mo, CoMo and NiMo supported KIT-6 material with γ-Al_2O_3 and SBA-15 supported analogues. Such a comparison is shown in Fig. 16. In the same figure, oxygen uptakes on these catalysts are also shown. A significant support effect can be noticed for KIT-6 when compared to γ-Al_2O_3 and SBA-15. KIT-6 supported catalysts are 2–3 times more active than γ-Al_2O_3 and nearly 1.5–2 times more active than SBA-15 supported catalysts for both HDS and HYD functionalities. 3-D pore connectivity as well as large surface area and pore volume are the major factors for the significant improvement in the activity over KIT-6 support.

4. Conclusion

KIT-6 silica with well-ordered 3-D mesoporosity is very effective support for Mo, CoMo and NiMo catalysts prepared by incipient wetness impregnation method. TEM and low-angle XRD analyses indicated that the cubic Ia3d mesostructure is retained after Mo and promoter incorporation. The wide-angle XRD (as well O_2-chemisorption analysis) indicated that MoO_3 (and MoS_2) is likely to be present in highly dispersed state up to 8 wt.% Mo and the crystallite size is <40 Å. The IR spectral studies gave clear evidence for the presence of octahedral and tetrahedral molybdenum and its growth with Mo loading. TPR studies revealed a twin peak reduction pattern, which can be attributed to the reduction of octahedral and tetrahedral molybdenum species.

The oxygen chemisorption analysis indicated that the formation of patchy monolayer of MoS_2 on the surface completes around 8 wt.% Mo. Calculated crystallite sizes indicate three-dimensional growth of MoS_2 at higher loadings. The catalytic activities for HDS and HYD correlated well with the oxygen chemisorption. A linear correlation is obtained between catalytic activities and oxygen uptakes suggesting that the increase in anion vacancies is indeed responsible for the observed variation of HDS and HYD activities. A comparison with γ-Al_2O_3 and SBA-15 supported catalysts shows superior activities of KIT-6 supported catalysts. This higher activity is attributable to 3-D mesopore connectivity resulting in better catalyst dispersion, higher reducibility of Mo, and faster diffusion of reactants and products in case of KIT-6 supported catalysts.

Acknowledgements

KS and SG thank CSIR, New Delhi, India, for Research Fellowship. AKS acknowledges DST, India for a Fast Track Young Scientist Award.

Appendix A. Supplementary data

Supplementary data associated with this article can be found, in the online version, at doi:10.1016/j.apcatb.2009.02.010.

References

[1] C. Song, Catal. Today 86 (2003) 211.
[2] Y. Okamoto, M. Breysse, G.M. Dhar, C. Song, Catal. Today 86 (2003) 1.
[3] G. Murali Dhar, B.N. Srinivas, M.S. Rana, M. Kumar, S.K. Maity, Catal. Today 86 (2003) 45.
[4] M. Breysse, P. Afanasiev, C. Geantet, M. Vrinat, Catal. Today 86 (2003) 5;
H. Guo, Y. Sun, R. Prins, Catal. Today 130 (2008) 249;
B. Yoosuk, J.H. Kim, C. Song, C. Ngamcharussrivichai, P. Prasassarakich, Catal. Today 130 (2008) 14;
Z.X. Yu, L.E. Fareid, K. Moljord, E.A. Blekkan, J.C. Walmsley, D. Chen, Appl. Catal. B 84 (3–4) (2008) 482;
H. Hamdy, Appl. Catal. B 84 (1–2) (2008) 1.
[5] S.K. Maity, B.N. Srinivas, V.V.D.N. Prasad, A. Singh, G. Murali Dhar, T.S.R. Prasada Rao, in: T.S.R. Prasada Rao, G. Murali Dhar (Eds.),Recent advances in basic and applied aspects of industrial catalysis, Stud. Surf. Sci. Catal. 113 (1998) 579.
[6] R. Prins, V.J.H. de Beer, G.A. Somsserjai, Catal. Rev. Sci. Eng. 31 (1989).
[7] L.C. Caero, A.R. Romero, J. Ramirez, Catal. Today 78 (1–4) (2003) 513.
[8] M.C. Barrera, M. Viniegra, J. Escobar, M. Vrinat, J.A. de los Reyes, F. Murrieta, J. García, Catal. Today 98 (1–2) (2004) 131.
[9] S.K. Maity, M.S. Rana, B.N. Srinivas, S.K. Bej, G. Murali Dhar, T.S.R. Prasada Rao, J. Mol. Catal. A: Chem. 153 (1–2) (2000) 121.
[10] G. Murali Dhar, F.E. Massoth, J. Shabtai, J. Catal. 85 (1994) 44.
[11] S. Damyanova, L. Petrov, M.A. Centeno, P. Grange, Appl. Catal. A: Gen. 224 (1–2) (2002) 271.
[12] M.S. Rana, E.M.R. Capitaine, C. Leyva, J. Ancheyta, Fuel 86 (9) (2007) 1254.
[13] M.S. Rana, S.K. Maity, J. Ancheyta, G. Murali Dhar, T.S.R. PrasadaRao, Appl. Catal. A: Gen. 268 (1–2) (2004) 89.
[14] F.E. Massoth, G. MuraliDhar, J. Shabtai, J. Catal. 85 (1994) 52.
[15] F.P. Daly, H. Ando, J.L. Schmitt, E.A. Sturm, J. Catal. 108 (1987) 401.

[16] M.S. Rana, B.N. Srinivas, S.K. Maity, G. Murali Dhar, T.S.R. PrasadaRao, J. Catal. 195 (2000) 31.
[17] W. Zhaobin, X. Qin, G. Xiexian, E.L. Sham, P. Grange, B. Delmon, Appl. Catal. 75 (1991) 179.
[18] D. Li, A. Nishijima, D.E. Morris, J. Catal. 182 (2) (1999) 339.
[19] W.J.J. Welters, G. Vorbeck, H.W. Zandbergen, J.M. van de Ven, E.M. van Oers, J.W. de Haan, V.H.J. de Beer, R.A. van Santen, J. Catal. 161 (2) (1996) 819.
[20] A. Wang, Y. Wang, T. Kabe, Y. Chen, A. Ishihava, W. Qian, P. Yao, J. Catal. 210 (2002) 319.
[21] T. Klimova, M. Calderon, J. Ramirez, Appl. Catal. A: Gen. 240 (2003) 29.
[22] A. Wang, Y. Wang, T. Kabe, Y. Chen, A. Ishihara, W. Qian, J. Catal. 199 (2001) 19.
[23] U.T. Turaga, C. Song, Catal. Today 86 (2003) 129.
[24] T. Chiranjeevi, P. Kumar, M.S. Rana, G. Murali Dhar, T.S.R. PrasadaRao, J. Mol. Catal. A: Chem. 181 (2002) 109.
[25] G. Murali Dhar, G. Muthu Kumarana, Manoj Kumara, K.S. Rawat, L.D. Sharma, B. David Raju, K.S. Rama Rao, Catal. Today 99 (2005) 309.
[26] L. Vradman, M.V. Landau, M. Herskowitz, V. Ezersky, M. Talianka, S. Nikitenko, Y. Koltypin, A. Gedanken, J. Catal. 213 (2003) 163.
[27] G. Muthu Kumaran, Shelu Garg, Kapil Soni, Manoj Kumar, L.D. Sharma, G. MuraliDhar, K.S. RamaRao, Appl. Catal. A: Gen. 305 (2006) 123.
[28] G. Muthu Kumaran, Shelu Garg, Kapil Soni, Manoj Kumar, L.D. Sharma, K.S. Rama Rao, G. Murali Dhar, Ind. Eng. Chem. Res. 46 (2007) 4747.
[29] T. Chiranjeevi, P. Kumar, S.K. Maity, M.S. Rana, G. Murali Dhar, T.S.R. Prasada Rao, Micropor. Mesopor. Mater. 44–45 (2001) 547.
[30] K.M. Reddy, B. Wei, C. Song, Catal. Today 43 (1998) 261–272.
[31] A. Sampieri, S. Pronier, J. Blanchard, M. Breysse, S. Brunet, F. Flyerwerg, C. Louis, G. Parot, Catal. Today 107–108 (2005) 537.
[32] A. Corma, A.V. Martinez, M. Soria, J.B. Monton, J. Catal. 153 (1995) 25.
[33] Freddy Kleitz, Shin HeiChoi, Ryong Ryoo, Chem. Commun. (2003) 2136.
[34] B.S. Parekh, S.W. Weller, J. Catal. 47 (1977) 100.
[35] B.E. Concha, C.H. Bartholomew, J. Catal. 79 (1983) 327.
[36] G. Murali dhar, B.E. Concha, G.L. Bartholomew, C.H. Bartholomew, J. Catal. 89 (1984) 274.
[37] K.S.P. Rao, H. Ramakrishna, G. Murali Dhar, J. Catal. 133 (1992) 146.
[38] X. Liu, B. Tian, C. Yu, F. Gao, S. Xie, B. Tu, R. Che, L. Peng, D. Zhao, Angew. Chem. Int. Ed. 41 (2002) 3876.
[39] F. Prinetto, G. Cerrato, G. Ghiottiand, A. Chiorino, J. Phys. Chem. 99 (1995) 5556.
[40] R. Thomas, J.A. Moulijn, V.H.J. de Beer, J. Medema, J. Mol. Catal. 8 (1980) 161.
[41] S.R. SeyedMonir, R.F. Howe, J. Catal. 110 (1988) 216.
[42] Tuan-chi Liu, J. Michel Forissier, Gishle Coudurier, Jacques C. VCdrine, J. Chem. Soc., Furaday Trans. I 85 (7) (1989) 1607–1618.
[43] I.E. Wachs, F.D. Hardcastle, S.S. Chan, Spectroscopy 1 (1986) 30.
[44] R. Lopez Cordero, A. Lopez Agudo, Appl. Catal. A: Gen. 202 (2000) 23.
[45] R. Lopez crodero, F.J. GillLlambias, A. Lopez Agudo, Appl. Catal. 74 (1991) 125.
[46] S. Demyanova, A. Spozakina, K. Jiratova, Appl. Catal. A: Gen. 125 (1995) 257.
[47] H. Xiong, Y. Zhang, W. Wang, Li, J. Catal. Commun. 6 (2005) 512–516.
[48] H. Topsoe, B.S. Clausen, F.E. Massoth, in: J.R. Anderson, M. Baudart (Eds.), Hydro-Treating Catalysis-Science and Technology, vol. 11, Springer-Verlag, New York, 1996.